Bulletin of Earthquake Engineering
https://doi.org/10.1007/s10518-026-02591-w

ORIGINAL ARTICLE

Study on the fragility assessment of existing reinforced concrete buildings considering ageing processes

Julia Eberl[1] · **Alexander Stark**[1]

Received: 17 April 2025 / Accepted: 9 July 2026

Abstract

A common method for estimating building damage is the use of fragility functions. When developing fragility curves, it is essential to consider the specific characteristics, i.e. the age and changes over the lifetime, to ensure a reliable damage assessment. Existing buildings are more vulnerable to the effects of ageing due to their lower material strengths and concrete covers. This paper analyses the impact of corrosion and pre-damage on the fragility curves for existing buildings with a developed multiscale approach. Considering the consequences of corrosion, three effects are taken into account: reduction of reinforcement cross-section, reduction of steel ductility, and deterioration of concrete. For the pre-damage, a sequence of loading and unloading is simulated. The analysis focuses on a reinforced concrete building constructed in 1943, initially in its original state, with particular attention to its original material and reinforcement properties, and under the impact of corrosion attack after 80 years as well as pre-damage. A moderate corrosion attack can result in a 64% reduction in the overall shear base and an increase in fragility of up to 33% compared to a new building from 2023. The analysis of pre-damage has been demonstrated to result in a maximum increase of 18% in the probability of exceedance, contingent on the extent of pre-damage. The utilisation of fragility curves, developed for new buildings, results in a substantial underestimation of vulnerability when applied to existing structures.

Keywords Fragility functions · Corrosion · Pre-damage · Reinforced concrete · Existing buildings · Ageing

✉ Julia Eberl
julia.eberl@kit.edu

Alexander Stark
alexander.stark@kit.edu

[1] Institute of Concrete Structures and Building Materials, Karlsruhe Institute of Technology, Gotthard-Franz-Strasse 3, 76131 Karlsruhe, Germany

Published online: 17 July 2026

1 Introduction

Earthquakes are infrequent but catastrophic natural disasters with a high potential to cause significant damage and loss of life. Their severe impact on the population and infrastructure of the affected area gives rise to significant social and economic consequences. Earthquakes accounted for a mere 8% of natural disaster occurrences worldwide during the period from 2000 to 2019 (Centre for Research on the Epidemiology of Disasters and United Nations Office for Disaster Risk Reduction 2020). However, a detailed analysis of fatalities according to disaster category reveals that 58% of the 1.23 million fatalities (2000–2019) were attributable to earthquakes, representing the highest proportion. The deadliest natural disaster worldwide during this period was the earthquake and related tsunami in the Indian Ocean in 2004, in which 226.408 people lost their lives. Furthermore, of the economic losses caused by natural disasters recorded between 2000 and 2019, earthquakes account for 21% (Centre for Research on the Epidemiology of Disasters and United Nations Office for Disaster Risk Reduction 2020).

Accordingly, the development of strategies to minimise the risk of earthquakes represents a primary focus of earthquake engineering. This encompasses the prediction of damage prior to an earthquake as well as the assessment of damage immediately following one. In the aftermath of an earthquake, a timely and reliable damage assessment is essential for the effective planning of rescue and evacuation operations and the efficient allocation of limited human and material resources (Kohns et al. 2025). In addition, accurate damage classification is important for assessing stability and identifying deficiencies that play an important role in aftershocks and subsequent earthquakes (Raghunandan et al. 2015; Wen et al. 2017).

Assessing damage caused by natural disasters is traditionally a manual process, requiring significant time and resources from on-site experts. As part of a research project, a trans- and interdisciplinary concept for the assessment and classification of earthquake damage was developed (Kohns et al. 2025; Zahs et al. 2023). This concept is composed of two sequential steps. Firstly, an initial damage calculation is performed based on fragility functions and building information. Subsequently, a damage classification is carried out based on unmanned aerial vehicle (UAV) data using machine learning and crowdsourcing methods. The system has been designed to enable efficient and timely damage assessment by integrating the strengths of domain knowledge in earthquake engineering, automated computational methods, and crowdsourcing (Kohns et al. 2025; LOKI Project Team, 2023a,b).

An important aspect of the concept and a common method for estimating building damage is the use of fragility functions (Crowley et al. 2021a, b; Ayala et al. 2015; Martins and Silva 2021; SYNER-G 2011). Fragility functions are a means of describing the probability of a structure exceeding a designated damage grade in relation to an earthquake intensity measure. The utilisation of fragility functions for a range of building classes (Brzev et al. 2013; Silva et al. 2018) in conjunction with experienced earthquake ground motions facilitates the fast calculation of an initial estimate of the anticipated building damage in the immediate aftermath of an earthquake (Kohns et al. 2025).

In developing fragility curves for a given target site, two important issues need to be considered: (1) the existing building typologies and structures, varying the materials and construction techniques according to the year of construction and the seismic code, and (2) the changes in characteristics over the lifetime of the structure for example due to ageing and damage. In summary, it is essential to take into account the current characteristics, i.e. the initial characteristics as a function of the year of construction as well as the changes over the lifetime up to the point of investigation, to ensure a reliable damage assessment (Eberl 2025). Temporal changes have frequently been disregarded in the development of fragility curves (Silva et al. 2022). The frequent failure to take this into account is due, among other things, to the unknown input values, and the complexity of recording and generalising the effects of ageing to building classes. As the year of construction, the building's history and the exact material properties must be considered, the investigations for each building are highly specific. Consequently, fragilities and vulnerabilities have typically been determined only for the initial state of a new building. However, it is important to note that vulnerability can undergo significant changes over the lifetime of a building. Such changes can be attributed to various factors, including structural modifications, the addition of storeys, the deterioration of load-bearing capacity due to the accumulation of damage, and the effects of ageing (Silva et al. 2022). Environmental conditions such as temperature fluctuations and sulphates, as well as corrosion, have negative effects on material properties (Berto et al. 2020; Caprili et al. 2024). Damage caused by previous earthquakes also has a major influence on the seismic behaviour of a building (Raghunandan et al. 2015; Wen et al. 2017).

The authors proposed a multiscale approach to derive fragility functions for reinforced concrete (RC) structures based on a large number of numerical damage criteria to consider various possible damage patterns at different scales for five damage grades ranging from Slight to Destruction (Kohns et al. 2022). The approach is universally applicable for the development of fragility functions for individual buildings, general building classes, regional construction methods, material and system properties as well as different intensity measures (Eberl 2025). In Kohns et al. (2023), the approach developed to generate fragility curves is extended to include the effects of corrosion-related ageing by providing an example. The investigation focuses on new buildings and the potential future impact of corrosion. The study was based on initial conditions that met current standards, rather than on existing buildings.

The lower material strengths and concrete covers of existing buildings render them significantly more vulnerable to the effects of ageing. The present paper therefore analyses the impact of such effects on the fragility curves for existing buildings. In order to achieve this objective, the methodology for the ageing effects and the development of the fragility curves, as well as the characteristics of the sample buildings, are described in the first instance. The subsequent presentation of results is accompanied by visualisation through the utilisation of a sample of streets and houses, and these results are then discussed.

2 Methods

The proposed multiscale approach to develop fragility functions employs various numerical criteria at different scales to determine the positions of five damage grades ranging from Slight to Destruction on the building's response curve (Kohns et al. 2022). These criteria include both global and material-specific characteristics and are assigned to the five damage grades based on their frequency and distribution. Further details can be found in Kohns et al. (2022). The approach developed in this study demonstrates a superior capacity to recognise diverse forms of damage at various levels in comparison to existing methodologies that employ displacement criteria exclusively.

In Kohns et al. (2023), corrosion-related ageing effects are included in the multiscale approach to demonstrate the change of the developed fragility functions for a new RC building. The effects of corrosion on steel and concrete are taken into account both in the material laws and in the damage criteria. The pushover curves for a new building after 80 years, incorporating the effects of corrosion, demonstrate a decline in maximum base shear of up to 13%, with damage grades manifesting at reduced displacements compared to the initial state. The modification of input parameters leads to a change in fragility curves, resulting in an enhancement of probabilities of exceedance by up to 25%. As a next step and further development, in this paper, existing buildings are investigated.

2.1 Effects of rebars corrosion on structural behaviour

In this paper, existing buildings are studied as the effects of ageing have an even greater influence on the fragility functions due to lower material strengths and concrete covers. The following three effects are considered in relation to the consequences of corrosion: (1) The reduction of the cross-section of the longitudinal/transverse reinforcement, (2) the reduction of the ductility of the steel or the final deformation of the reinforcing bars, and (3) the deterioration of the concrete strength or concrete cover.

(1) In the case of chloride-induced corrosion, the reduction of the cross-section of the reinforcing steel is localised, whereas in the case of carbonation, the cross-sectional loss is more extensive. This phenomenon ultimately leads to a reduction in the component's resistance and load-bearing capacity. According to Berto et al. (2009), the reduction in the diameter of a corroding reinforcing bar after the time t (in years) can be estimated using the following Eq. (1):

$$\phi\ (t) = \ \phi_0 - 2P_x = \ \phi_0 - 2i_{corr}\kappa\ (t - t_{in}) \tag{1}$$

The function ϕ(t) describes the residual diameter at the time t, with ϕ_0 representing the nominal diameter, t_{in} the start of corrosion on the surface of the rebar (initiation time in years) and P_{x} the average value of the corrosion attack penetration in the form of diameter loss. This attack penetration can be defined as the product of i_{corr} as corrosion current density, κ=0.0116 as a conversion factor of μA/cm^2 into mm/year for steel and the period ($t-t_{\mathrm{in}}$), in which the corrosion takes place (propagation time in years). The factor 2 in Eq. (1) represents uniform steel loss due to carbonation and may reach up to 10 in cases of chloride-induced pitting corrosion (Simioni 2009). The presented investigation focuses on uniform steel loss resulting from carbonation. More details can be found in Eberl (2025); Berto et al. (2009); Simioni (2009); Berto et al. (2020).

(2) Reinforcement corrosion also changes the mechanical properties of the steel (Apostolopoulos and Papadakis 2008; Berto et al. 2009; Coronelli and Gambarova 2004; Pitilakis et al. 2014; Simioni 2009). The reduction of the elongation at maximum load and the ultimate deformation is mainly determined experimentally (Apostolopoulos and Papadakis

2008; Berto et al. 2009; Rodriguez et al. 1997). Corrosion reduces the ductility, leading to a more brittle failure. In Rodriguez and Andrade (2001), the resulting values are 30% and 50% reduction in elongation at maximum load for losses of steel section of 15% and 28% respectively. Values in between can be calculated by linear interpolation. The values are used, for example, in Pitilakis et al. (2014); Simioni (2009); Rodriguez and Andrade (2001). These values form the basis for this investigation.

(3) The increase in volume of the corrosion products on the rebar surface creates a radial pressure on the surrounding concrete. In cases that tensile stresses in the concrete exceed its tensile strength, the potential consequences may encompass the formation of cracks in the concrete cover, the detachment of the outer concrete layers, or the complete loss of the concrete cover. The concrete cover is particularly vulnerable to corrosion due to carbonation, and various approaches can be found in the literature regarding the corrosion-induced concrete damage. One such approach, as outlined in Rodriguez and Andrade (2001), involves reducing the concrete cross-section by the concrete cover. Furthermore, numerous studies have been conducted on adapting the concrete constitutive relationship with a reduction in compressive strength and assuming a more brittle post-peak behaviour (Capozucca and Cerri 2003; Coronelli and Gambarova 2004; Simioni 2009; Vecchio and Collins 1986; Yalciner et al. 2012). The approach proposed by Vecchio and Collins (1986) is employed in this study. This approach was developed independently of standardisation and is used in Coronelli and Gambarova (2004); Yalciner et al. (2012); Caprili et al. (2024). The reduced concrete strength f_c* is calculated using the following Eq. (2):

$$f_c^* = \frac{f_c}{1 + K \cdot \frac{\epsilon_1}{\epsilon_{c0}}} \tag{2}$$

where $K=0.1$ as a coefficient for medium-diameter ribbed bars, ε_{c0} as strain at the peak compressive stress, and ε_1 as average (smeared) tensile strain in the cracked concrete at right angles to the direction of the applied compression. The strain ε_1 is calculated from the ratio of the width increased by corrosion cracks to the original section width (Yalciner et al. 2012; Coronelli and Gambarova 2004). This ratio can be estimated using the number of compressed rebars and the crack width, referring to Yalciner et al. (2012); Coronelli and Gambarova (2004).

2.2 Characteristics of the analysed building

When analysing existing buildings, it is necessary to consider the initial conditions, which vary depending on the year of construction and the prevailing standards of the era. Key differences include the compressive strength of the materials used, such as concrete and steel, the quantity of reinforcement, the width of concrete cover, and the type and length of anchorage. For instance, a reduced concrete cover can lead to a decreased initiation time, thereby amplifying the corrosion effect for a given building age. This can result in an increased fragility of the structure.

The subsequent analysis will consider a German sample building, assuming that it is analysed in 2023 being 80 years old, i.e. it was constructed in 1943. As a point of initial state and reference, a regular four-storey RC frame building is employed, as previously outlined in Kohns et al. (2022) and Kohns et al. (2023). The three-dimensional model is shown in Fig. 1 (A). It is assumed that the standard used is DIN 1045 in its 1937 version (Deutscher Ausschuss für Eisenbeton 1937). The assumption is made that the concrete is of high quality, with a cube compressive strength of at least 15.7 N/mm² after 28 days. The conservative strength class C16/20 is assumed (Table 1), although a significantly lower strength class would also be conceivable. The modulus of elasticity of the concrete equals 13.700 N/mm² (Table 1). The minimum concrete cover required for components intended for outdoor use is 20 mm, while in other cases, a lower concrete cover is acceptable. The reinforcement is also conservatively assumed to be made of higher-quality steel to match the higher-quality concrete. The minimum yield strength of this material is 353 N/mm² for diameters up to 18 mm and 343 N/mm² for diameters between 19 mm and 30 mm. Consequently, a yield strength of 353 N/mm^2 is conservatively calculated (Table 1). Related is an elongation at break of 20%

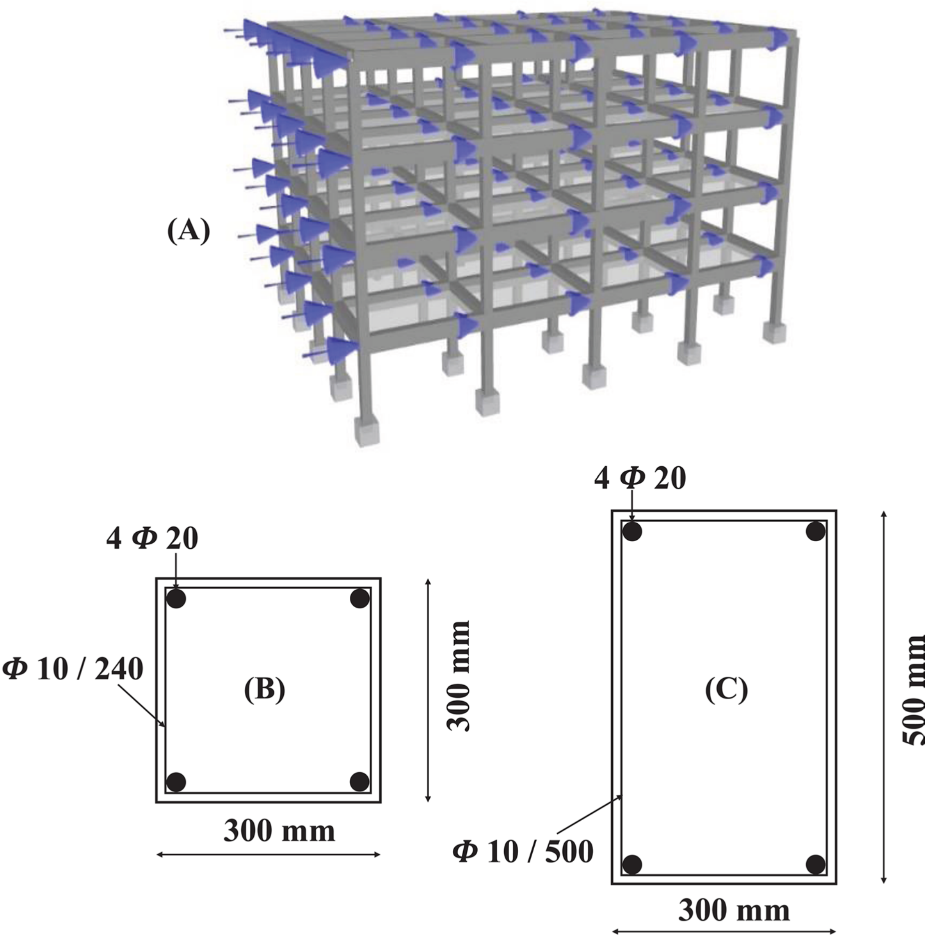

Fig. 1 3D model (**A**), sections and reinforcement of columns (**B**) and beams (**C**) of the analysed building from 1943

Table 1 Characteristics of the analysed building from 1943

Characteristics of the unaged building	Value
Concrete strength class	C16/20
Concrete modulus of elasticity	13.700 N/mm²
Concrete cover	20 mm
Reinforcement yielding strength	353 N/mm^2
Ratio modulus of elasticity of steel and concrete	15
Characteristics of the aged building following 80 years of corrosion exposure	Value
Diameters reinforcement	18.75, 10.75, 8.75 mm
Average reduction in elongation	35.3%
Reduced concrete strength	6.93 N/mm^2

on the long and 24% on the short proportional bar. The ratio of the modulus of elasticity of steel and concrete is 15 (Deutscher Ausschuss für Eisenbeton 1937).

In addition to the material properties, the reinforcement ratio is adapted to the applicable standard. The reinforcement diameters are chosen in the same way as in the reference model. The determination of the moments of continuous beams is to be conducted in accordance with the established principles for the analysis of freely rotating continuous beams (Deutscher Ausschuss für Eisenbeton 1937). In the calculation of the internal forces, moments of a maximum of 30 kNm result from the floor loading following the reference building. The employment of contemporary calculation methodologies, incorporating the adjusted material parameters, yields a low reinforcement requirement of 0.4 cm^2. A minimum reinforcement ratio is not required according to DIN 1045–1937. Therefore, longitudinal reinforcement in the beams is provided by two rebars with a diameter of 20 mm each, used as upper and lower reinforcement (cf. Fig. 1 (C)). Taking into account the vertical load according to the reference model, which can be assumed to be conservative compared to the loads from 1943 results in a maximum shear force in the beam of 43.16 kN. With a width of 0.3 m and an inner lever-arm of 0.4 m, this results in a maximum shear stress of 0.35 N/mm^2. This shear stress is less than 0.4 N/mm^2, so that DIN 1045–1937 does not require stirrup reinforcement to absorb the shear stress. However, the interaction of the tension and compression chord must be ensured. It is assumed here that only a small number of stirrups are installed. Therefore, the spacing of the stirrups (10 mm diameter) in the model is set to 500 mm (cf. Fig. 1 (C). An increase in the load-bearing capacity due to confinement effect is not assumed, as this is not permitted for rectangular stirrups. For the columns, the allowable total load is equated to the maximum normal force in the columns of 627 kN. Utilising the values of 16 N/mm^2 for the compressive strength of the concrete, 0.09 m^2 for its cross-sectional area, and 353 N/mm^2 for the steel's stress, the requisite reinforcement is determined to be 12.25 cm^2. The selection of four 20 mm diameter bars for the columns results in an area of 12.6 cm^2 (cf. Fig. 1 (B). However, the eccentric pressure equation yields a substantially lower amount of reinforcement, thus being inconclusive. The interpolated minimum ratio of longitudinal reinforcement is 0.7%, with a ratio of $l/h = 2.5/0.3 = 8.3$. The existing longitudinal reinforcement ratio is 1.4%, which means that both the minimum and maximum reinforcement ratios are satisfied. The requirements for the maximum stirrup spacing in the columns give a maximum stirrup spacing of 240 mm (10 mm diameter) for a diameter of 20 mm of longitudinal reinforcement (cf. Fig. 1 (B). It should be noted that no increase in the load-bearing capacity of the columns may be taken into account as a result of the confinement. Deutscher Ausschuss für Eisenbeton (1937).

The modelling of the columns and beams is conducted in SeismoStruct (Seismosoft 2023) through a simplified approach, employing infrmFBPH elements (inelastic plastic-hinge force-based frame elements). These elements are characterised by their ability to concentrate inelasticity at the two ends of the element within a fixed length of the element. The beams are modelled from column to column, meaning that both the upper and lower bending tensile reinforcement is continuously applied. This configuration precludes the possibility of arranging the reinforcement exclusively in the tension zone and addressing the curtailment of longitudinal tension reinforcement. Consequently, the construction method remains unaltered from the reference building to ensure the comparability of the results.

The Eqs. (1) and (2), as well as the experimental values for the reduction in elongation at maximum load (Rodriguez and Andrade 2001), are utilised to calculate the material properties for the aged structure following 80 years of corrosion exposure (Table 1). For a moderate corrosion attack (e.g. average chloride exposure, humid climate), the value of the corrosion current density is set to i_{corr} = 0,8 µA/cm^2 (Berto et al. 2009). The initiation time is conservatively assumed to be 12.6 years (Berto et al. 2009), as no more precise information is available.

The diameters 20 mm, 12 mm and 10 mm are reduced to 18.75 mm, 10.75 mm and 8.75 mm (Eq. 1). To account for the smooth steel, the parameter A2 is set to 0.001 (Cosenza et al. 2010) in the Menegotto-Pinto constitutive relationship (Menegotto and Pinto 1973; Seismosoft 2023). The average reduction in cross-sectional area of 18.44% results in an average reduction in ductility of 35.30%. This reduction in ductility leads to a decrease in the maximum steel elongation and the damage criterion for steel failure. The concrete strength is reduced from 16 N/mm^2 to 6.93 N/mm^2 and the strain criterion for spalling of the concrete cover is reduced to 0.0017. The tensile strength of the concrete is not considered in the standard, so a negligible value of $1 \cdot 10^{-6}$ N/mm^2 is assumed.

2.3 Analysis of the building

The building from 1943 with the material properties and reinforcement according to DIN 1045–1937 (Deutscher Ausschuss für Eisenbeton 1937) is analysed in the initial state as well as after 80 years under corrosion attack.

The numerical analysis is conducted using the SeismoStruct software (Seismosoft 2023). In each case, four pushover analyses are carried out. The pushover analysis is conducted for the two directions x and y. Due to the symmetry of the building, there is no difference between the positive and the negative orientation for x and y, respectively. Two different lateral load patterns are investigated, a uniform and a modal distribution. For the modal distribution, an eigenvalue analysis is run before the pushover analysis to determine the load pattern for the modal shape with the highest effective modal mass percentage for each direction. Specific horizontal loads for each node are defined as incremental loads in the relevant direction (cf. Fig. 1 (A)). In total, for each point of time, there are four analyses conducted, each up to a displacement of the control node of 0.25 m in 100 steps. As control node, the node on the top floor in the centre is chosen.

The multiscale criteria are utilised to ascertain the damage grades on the pushover curves, with the criterion exhibiting the lowest displacement proving to be decisive. The spectral displacement limit values are subsequently derived from this. The pushover curves of the MDoF system simulated with SeismoStruct (Seismosoft 2023) are transformed into the SDoF system curves in the ADRS format and approximated as capacity curves. The fragility functions are developed with VMTK (Martins et al. 2021) using the computed pushover curves and derived damage grades limit values. As ground motion records, over 2000 records of the Engineering Strong Motion Database (ESM) (Luzi et al. 2015) for Europe are selected as input (uncorrected and unscaled). Peak ground acceleration (PGA) is chosen here as traditional intensity measure (IM), however, Eberl (2025) demonstrated that this approach can also be applied to other IMs, such as Sa(T). Further information about the procedure for determining the damage grades and the fragility curves can be found in Kohns et al. (2022); Eberl (2025).

3 Results

3.1 Results of the analysis of the building

The following section presents the results of the investigation of the existing 1943 building. The pushover curves for the *x*-direction with modal horizontal load distribution are shown as an example in Fig. 2.

The decrease in the total base shear for the analysed existing building between 0 and 80 years, i.e. without and with corrosion, is approximately 41% (1475 kN to 875 kN). As an additional comparison, the reference building from 2023 is shown as a black curve. This building has material properties (concrete C30/37, reinforcement B500B) in accordance with the current standard and is described in detail in Kohns et al. (2022). Compared to the new building in 2023, the 1943 building under the influence of corrosion after 80 years shows a reduction in the total base shear of 64% (2445 kN to 875 kN). Comparing the step numbers at which the criterion is exceeded for each analysis, it can be seen that the damage grades tend to occur at lower displacements when corrosion is taken into account. This shows that corrosion makes the building more fragile to damage. It can also be seen that the shape of the pushover curves changes under the influence of corrosion towards a

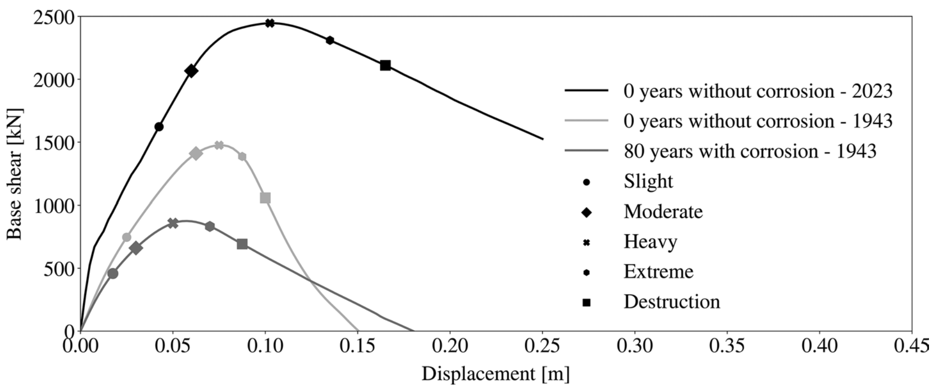

Fig. 2 Pushover curves for the *x*-direction with the modal horizontal load distribution and the associated damage grades for the analysed RC frame building from 1943 in its initial state and after 80 years under corrosion attack, as well as for the reference building from 2023

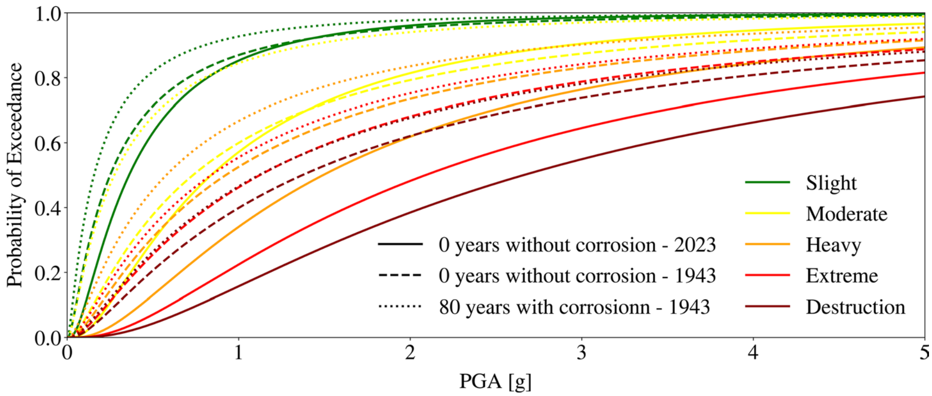

Fig. 3 Fragility curves for the five damage grades of the analysed RC frame building from 1943 in its initial state and after 80 years under corrosion attack, as well as for the reference building from 2023

Table 2 Distribution parameters of the lognormal distributions of the five damage grades of the analysed RC frame building from 1943 in its initial state and taking into account corrosion after 80 years and for the building from 2023 in its initial state

Age building[1]	Parameter [log g]	Damage grade				
		Slight	Moderate	Heavy	Extreme	Destruction
0–2023	mean	-1,020	-0,175	0,399	0,736	0,978
	standard deviation	0,973				
0–1943	mean	-1,384	-0,311	-0,079	0,116	0,315
	standard deviation	1,230				
80–1943	mean	-1,855	-1,293	-0,549	-0,176	0,110
	standard deviation	1,274				

[1]The first number denotes the age of the building in years, whilst the subsequent number indicates the year of construction

less steep load drop. The maximum displacement of 0.25 m can no longer be applied. The increased displacement capacity of the corroded model should be interpreted as a modelling effect rather than a real increase in ductility. The statements for the x-direction with modal horizontal load distribution, as previously outlined, apply by analogy to the other analyses carried out.

Figure 3 shows the fragility curves determined for the building in 1943 in its initial state (0 years without corrosion − 1943) and after 80 years under the influence of corrosion (80 years with corrosion − 1943). In addition, the fragility curves of the building from 2023 in the initial state (0 years without corrosion − 2023) are included for comparison. The associated distribution parameters of the lognormal distributions are presented in Table 2. It is evident that when corrosion is taken into account, the probability of damage increases for all damage grades, though the extent of this increase varies according to the specific damage grade. For an acceleration of 1.0 g, the probability of exceedance increases from 5.8% to 24.5% under the influence of corrosion alone, depending on the damage grade.

The extent of the increase for each damage grade depends on how the damage thresholds differ between the original and corroded buildings, influencing the calculation of exceedance probabilities. These thresholds are derived from the various damage criteria examined and depend on the criterion that is decisive for the respective damage grade. In comparison to the 2023 reference building, the fragility rises from 7.5% to 33%, contingent on the specific damage grade. The discrepancy exceeds 30% for all high damage grades.

The utilisation of fragility curves, which have been developed for new buildings, results in a substantial underestimation of vulnerability when applied to existing structures. This phenomenon can be attributed to two primary factors. Firstly, changes due to corrosion are not taken into account in the fragility curves, which is a crucial aspect as corrosion can significantly affect the structural integrity of a building. Secondly, there is high variability in the material properties and the ratio and layout of reinforcement, depending on the standard in the year of construction. In the presented case study, for a structure that was constructed 80 years ago, in 1943, this can result in a total reduction in base shear of up to 64% and an increase in vulnerability of up to 33% compared to a new building constructed in 2023.

3.2 Pre-damage as a further ageing effect

In addition to the issue of corrosion, another aspect of the ageing process that can occur throughout the building's service life is pre-damage caused by previous earthquakes. Strong main earthquakes are frequently succeeded by weak to moderate aftershocks, meaning that buildings are often exposed to a sequence of seismic events. Historical earthquakes have demonstrated that structures damaged by the primary earthquake are more prone to significant damage or destruction from subsequent aftershocks. The brief interval between the primary earthquake and the aftershock often does not permit adequate repair or restoration of the affected buildings (Raghunandan et al. 2015; Wen et al. 2017). Numerous studies have analysed damaged structures using single-degree-of-freedom (SDoF) systems (Amadio et al. 2003; Di Sarno 2013; Hatzigeorgiou and Beskos 2009; Zhai et al. 2014) and multi-degree- of-freedom (MDoF) systems (Abdelnaby and Elnashai 2015; Faisal et al. 2013; Hatzigeorgiou and Liolios 2010; Hosseinpour and Abdelnaby 2017; Jeon 2013; Jeon et al. 2015; Luco et al. 2004; Raghunandan et al. 2015; Ruiz-Garcia 2012; Ruiz-Garcia and Aguilar 2015) for modelling. The studies on different types of structures and different earthquake sequences (i.e. recorded or simulated earthquakes sequences) have a common conclusion that moderate aftershocks increase the damage to structures (Wen et al. 2017). In Luco et al. (2004), a comparison is made between static and dynamic computation of the residual capacity of a mainshock-damaged building to withstand an aftershock. In the static analysis, the building is first loaded and unloaded, resulting in an irreversible displacement. The building is then loaded again.

In this study, pre-damage is mapped as a result of loading and unloading. In SeismoStruct (Seismosoft 2023), a sequence of loading and unloading can be performed using displacement-controlled and force-controlled loading. Initially, displacement-controlled incremental loading of the building is conducted up to the displacement associated with the pre-damage level. The displacement values assigned to these levels are 0.5% for Slight, 1% for Moderate, 2% for Heavy, 3% for Extreme and 4% for Destruction. Subsequently, the building is unloaded through a force-based step, thereby maintaining an irreversible deformation. Finally, a displacement-based load is applied until the desired final displacement is reached.

The reference building is investigated under a sequence of loading and unloading. As previously outlined, pushover curves are determined, followed by the identification of the positions of the damage grades on these curves. It has been demonstrated that the irreversible displacement exhibits an increase with rising pre-damage grades, and moreover, the damage criteria that are achieved following unloading also undergo an increase. The occurrence of damage at lower displacements has been observed as the pre-damage grade increases.

The fragility curves for damage grades that exceed the pre-damage level are then derived from the capacity curves and the displacement limits (Fig. 4).

In comparison to fragility curves without pre-damage, the fragility increases for all damage grades. This difference increases with rising pre-damage grade, as evidenced by the shift of fragility curves to the left and the decrease in the mean of the lognormal probability distribution. As can be seen, the difference in probability of exceedance between the undamaged state and slight or moderate pre-damage is small. The curves for slight and moderate pre-damage are very close to each other. However, heavy and extreme pre-damage lead to a significant increase in fragility. This behaviour can be explained by the extent of irreversible displacements after unloading. Furthermore, the influence of pre-damage becomes more pronounced when the pre-damage level is closer to the respective final damage state. Overall, the probability of exceedance increases by up to 18%.

3.3 Visualisation of the results for a representative sample of streets and houses

In order to demonstrate a prototypical application of the determined results on the corrosion-related increase in fragility, 50 reinforced concrete buildings of different years of construction are analysed at different points in time (cf. Fig. 6). The fragility in the initial state is dependent on the year of construction of the building and the associated material properties. The increase in fragility due to corrosion is, in turn, dependent on the building analysed and the time of observation. The analyses are carried out every 10 years in the period from 1940 to 2020, with the values from analyses of three buildings for different years of construction used (1940, 1970 and 2020) and intermediate values interpolated. The buildings are all based on the reference building. The various initial material properties of the three buildings are taken into account based on their year of construction and the appli-

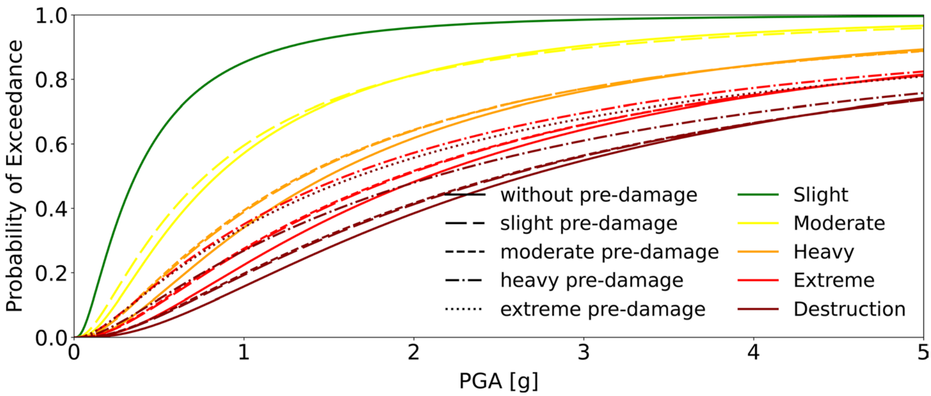

Fig. 4 Fragility curves for the five damage grades of the analysed RC frame building examined for aftershocks depending on slight to very severe pre-damage (displayed are damage grades that exceed the pre-damage level)

cable standard. Changes over time are also considered in the subsequent years' analyses. Some masonry buildings are also included in the street; however, these structures are not the subject of detailed analysis. Each building is assigned a house number and the year of its construction. The colours used in the figure correspond to the colour assignment listed in the legend: buildings without damage are shown in grey, while the colours green to dark red indicate the damage grade. Buildings that have not yet been realised are highlighted in white. In addition, the year of observation and the PGA analysed are noted in the top right-hand corner. The ground acceleration value of 1.0 g is selected as a value for regions characterised by high seismic activity.

Based on the fragility curves, each building has a probability distribution for the different damage grades depending on the peak ground acceleration. The sum of the probabilities of all damage grades, including the grade No damage, is 100%. The probability of occurrence for an individual damage grade is calculated by subtracting the probability of exceeding of the next higher damage grade. The result corresponds to the distance between the two fragility curves. This probability distribution changes over time under the influence of corrosion. This means that the building gets older and the effects of corrosion increase. In Fig. 5 the distributions of the probabilities of occurrence of the damage grades for a RC building constructed in 1940 are shown for the observation years 1940 to 2020.

It can be seen that under the influence of corrosion the likelihood of occurrence for No damage and the damage grade Slight decreases over time, while it increases for the damage grades Moderate to Destruction. The building thus becomes more fragile to high damage due to corrosion with increasing age. To apply this probability distribution to the specific sample of streets and buildings, the number of buildings per damage grade is chosen in proportion to the height of the corresponding bar for the associated year of construction and observation. For each year of construction, the distribution of damage grades in a given year of observation is divided into equidistant quantiles, whereby the number of quantiles corresponds to the number of buildings with the respective year of construction. The buildings from the respective year of construction are then randomly assigned to the quantiles. The buildings with lower or higher quantiles tend to have lower or higher damage grades, respectively. This can be interpreted to mean that for buildings with higher quantiles, other factors that are not taken into account in the fragility curves, such as the soil-structure interaction or the lower quality of the workmanship, lead to higher damage grades.

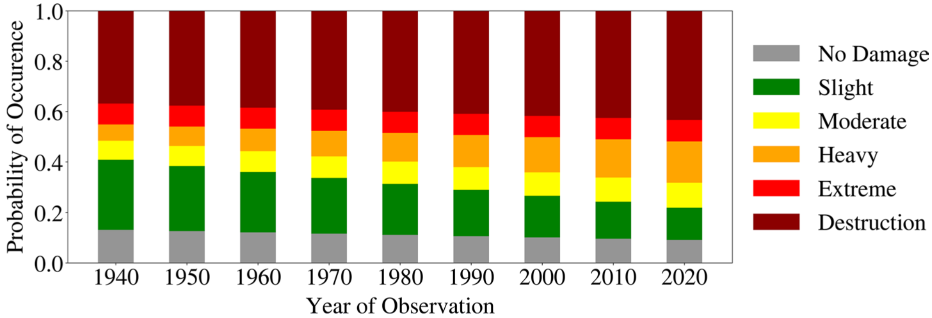

Fig. 5 Distribution of the probabilities of occurrence of the damage grades for a RC building constructed in 1940, for the observation years 1940 to 2020, under the influence of corrosion (PGA = 1.0 g)

Figure 6 shows the analysis and visualisation of the sample of streets and houses for a PGA of 1.0 g. All damage grades are already reached in the year of observation 1940 (Fig. 6 top left) due to the high ground motion. The highest damage grade Destruction is most frequently represented, which is reflected in the left-hand column of the probability distribution in Fig. 5. In the observation year 1960 (Fig. 6 top right), the damage grades for the buildings from 1940 increased. The buildings from the years 1950 and 1960 also show varying damage grades, although these tend to be lower than for the buildings from the year 1940. Of the total of 33 buildings, only three buildings show No damage. In the observation year 1980 (Fig. 6 bottom left), there is also an increase in the damage grades of existing buildings but new buildings tend to show less damage. By the observation year 2020 (Fig. 6 bottom right), the damage grades continue to increase and all damage grades are represented. The older buildings tend to have higher damage grades than the newer buildings.

The same analysis can also be carried out for a low peak ground acceleration of 0.1 g. It is evident from the findings that in 1940, the majority of buildings exhibited No damage, with only a few displaying slight damage. However, as time progresses, the extent of damage increases, reaching a point where by 2020, the damage grades No damage to Heavy are observed. This indicates an increase in the overall fragility of the buildings over time, although no major damage is anticipated at this ground motion. Furthermore, it is evident that older buildings are more vulnerable than newer ones.

A fragility index is derived from the visualisation of the vulnerability of the sample of streets and houses based on the damage grades. One point is awarded for each building without damage. The damage grades are assigned ascending points, with Slight corresponding to two points and Destruction to six points. This means that the change in the index over time includes both the increase in existing buildings and the increase in fragility. Figure 7 shows the increase in the number of buildings and the fragility index for the PGA = 0.1 g and 1.0 g in the period from 1940 to 2020.

The number of buildings has increased steadily over time, albeit not uniformly, reaching a maximum of 50. A notable increase in the number of buildings was observed in the construction years 1940 and 1950, as compared to later years. The fragility index for PGA = 0.1 g shows a course similar to that of the number of buildings, yet with a slightly more pronounced increase over time. This is evident from the greater distance between the two curves in the year 2020 compared to 1940. This indicates that not only new buildings are being constructed, but existing buildings are also becoming more vulnerable, consequently reaching a higher number of damage points. As the observation year increases, the curves flatten out, as fewer buildings are added and the newer buildings are less vulnerable. The fragility index exhibits a significant difference between 0.1 g and 1.0 g, indicating that structures are more vulnerable to damage at higher accelerations. Additionally, an increase in the fragility index for 1.0 g can be observed over time, as new structures are added and existing buildings become more vulnerable. The increase observed between 1940 and 2020 is more pronounced than that for 0.1 g, as the probability of high damage grades occurring increases more strongly.

In addition to the effects of corrosion, pre-damage can be incorporated into the application as a second aspect of ageing to be investigated. An earthquake can be assumed to occur at a certain point in time and the corresponding buildings can be subjected to a local increase in fragility due to the preliminary damage. In subsequent periods, the vulnerability increases continuously. Refurbishment can also be considered. For this purpose, the fragility of the

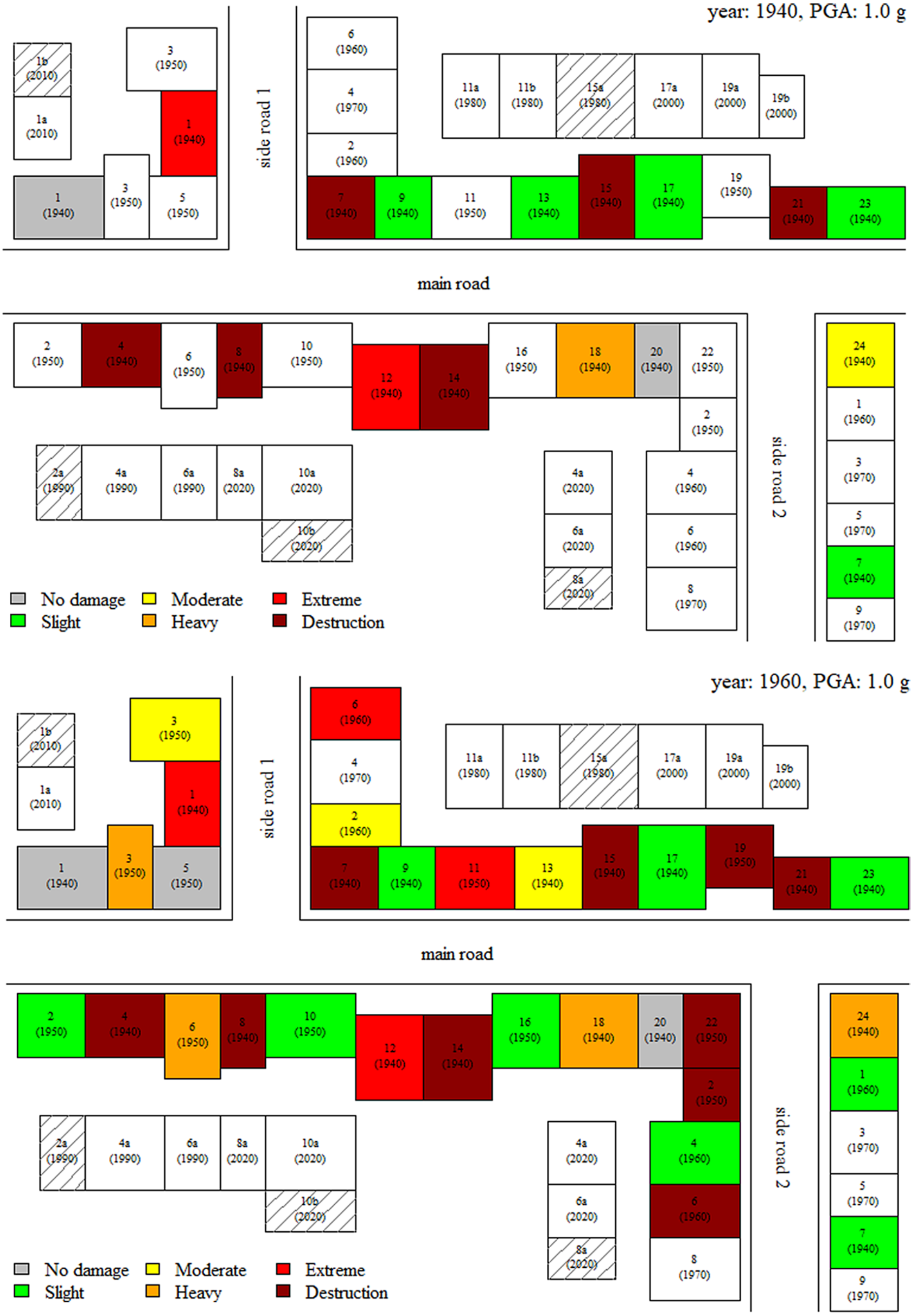

Fig. 6 Sample of streets with 50 RC buildings and five masonry buildings (hatched) for the observation years 1940, 1960, 1980 and 2020 and the associated damage grades (PGA = 1.0 g)

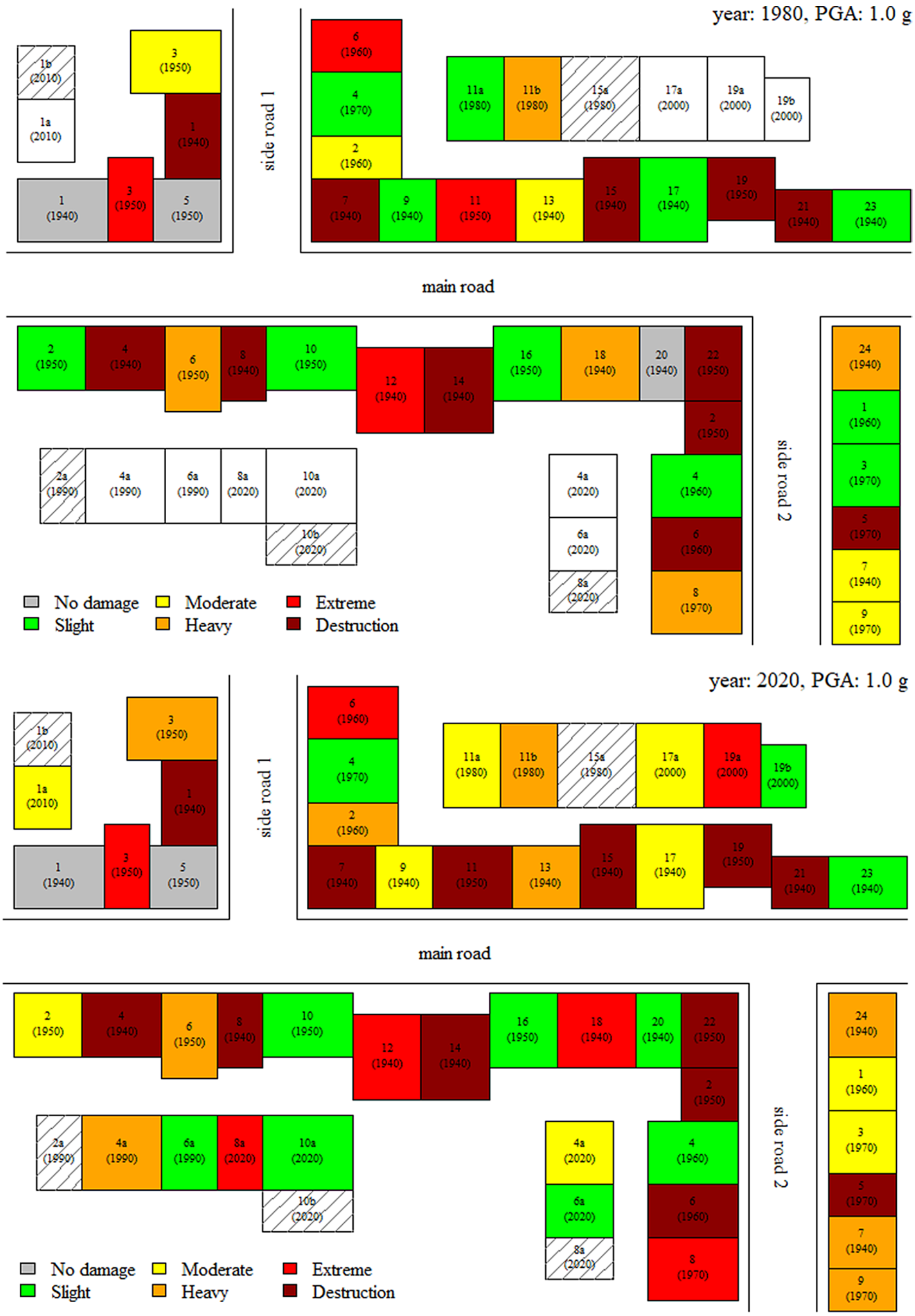

Figure 6 (continued)

refurbished buildings is selectively reduced at a defined point in time, provided that the refurbishment has an effect in this respect. In addition to the age-related increase in fragil-

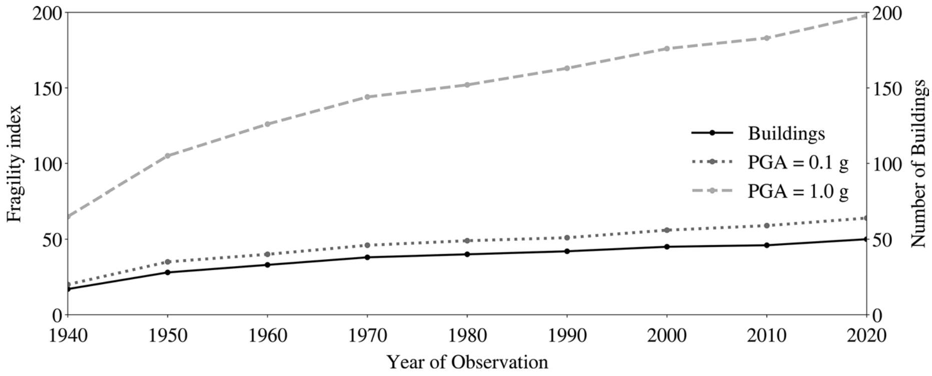

Fig. 7 Number of buildings and fragility index (PGA=0.1 g and 1.0 g) for the period from 1940 to 2020 for the sample of streets and buildings under investigation

ity, the potential for an earthquake also increases if no earthquake has occurred for a long period of time. The illustration, based on a sample of streets and buildings, visualises the significant increase in fragility of the buildings examined, particularly in the older existing buildings, and can be extended by further aspects.

4 Discussion

In the process of developing fragility curves for a given target site, it is of major importance to take into consideration the prevailing building typologies in that particular locale. In this regard, it is imperative to consider material and reinforcement properties depending on the year of construction and valid standards. Furthermore, the model must incorporate the effects of ageing, thereby ensuring the reliability of the resulting damage assessment. This paper demonstrates the applicability of the developed multiscale approach in analysing existing buildings, extending the scope to encompass ageing effects. In the case of the 1943 building, higher-quality material properties were assumed. The reinforcement detailing of RC buildings from the 1940s was highly variable and often characterized by smooth bars, limited anchorage, and non-ductile detailing. Due to modelling constraints, idealized reinforcement continuity and anchorage conditions were assumed. These simplifications may lead to an overestimation of ductility and an underestimation of seismic fragility. Therefore, the presented fragility curves should be interpreted as representative of an idealized configuration, while actual buildings of that period may exhibit even more brittle behaviour. In this example, it was initially assumed that all elements were subject to uniform corrosion. However, studies by Berto et al. (2009) and Simioni (2009), among others, have demonstrated that the spatial distribution of corrosion is important. Uneven corrosion can lead to torsion effects that negatively impact load-bearing behaviour. Studies conducted by the authors also revealed twisting of the floor plan when corrosion was considered for only one exterior wall of the building.

Due to the use of a range of modelling approaches and the consideration of different corrosion effects, a direct comparison of the results from the literature with each other and with the obtained results is only possible to a limited extent. Nevertheless, the achieved results are within the expected range according to the literature reviewed (Berto et al. 2009; Celarec et al. 2011; Pitilakis et al. 2014; Silva et al. 2022; Simioni 2009; Yalciner et al. 2012). The findings demonstrate the efficacy of the proposed methodology in accounting for damage and degradation effects at material, cross-section, and structure levels. The proposed multiscale approach, which uses damage criteria at different scales to relate all observed damage patterns to the seismic response of the building, considers various possible damage patterns at different scales more comprehensively than the well-known displacement criteria approach (Crowley et al. 2021a; Martins and Silva 2021). The exact results are case study-specific and not necessarily generalisable. The analysis of the various criteria facilitates the identification of the influence of material combinations, thereby enabling the determination of the material that is decisive, when a criterion is exceeded. Consequently, weak points in the system can be identified. The development of fragility curves can be conducted using any method, as the potential damage patterns are contained in the displacement limit values of the damage grades. The approach can be used to develop fragility functions for individual buildings, general building classes, region-specific construction methods, material and system properties, different intensity measures and properties that change over the lifetime of a structure.

The findings presented herein are compared with the outcomes of the investigations on new buildings under corrosion attack, which are documented in Kohns et al. (2023). It is evident that the impact of pure corrosion on the total shear base loss in older structures is more significant than in modern ones. To illustrate this point, the corrosion-induced decrease in the maximum total shear base after 80 years is 13% for the structure from 2023 to 28% for the building from 1943. Furthermore, the quality of workmanship in the construction of the buildings must be taken into account, since in some countries, the low quality of execution of construction projects can lead to a significant increase in fragility. Therefore, for example, a quality factor could be introduced whose value varies depending on the quality of execution. The factor is applied to the mean and the standard deviation of the lognormal probability distribution, and as a result, the curve would shift towards a higher fragility with lower acceleration in the event of deficiencies in execution. Alternatively, the deficiencies can be incorporated into the modelling process, for instance, through the exclusion of individual reinforcement stirrups or a reduced concrete strength.

The findings of the investigations carried out on pre-damage are in comparable ranges to those documented in the literature (Jeon 2013) and demonstrate that pre-damage can significantly increase fragility. The approach developed to take pre-damage into account by loading and unloading is not comprehensive, in the sense that it does not incorporate direct cyclic changes at the material level. Consequently, no fatigue symptoms are included in the approach. This implies that material degradation caused by a large number of previous load cycles cannot be recognised. The application is therefore only expedient for low-cycle fatigue. Conversely, for a substantial number of cycles characterised by high amplitudes (i.e., strong earthquakes), failure in the area of damage accumulation is a distinct possibility. This phenomenon must be modelled accordingly.

The street-based illustration shows the significant increase in vulnerability of the buildings studied, particularly the older existing buildings. This shows that the change in fragility of buildings, streets or whole areas over time should not be underestimated and should be taken into account in local authority assessments. When modelling real streets, it is important to remember that there are different classes of buildings with different characteristics.

The configuration of the buildings must also be taken into account as, for example, terraced houses have different load-bearing characteristics and the buildings can influence each other in the event of damage. The results can be incorporated into existing exposure models and automated to provide estimates of the change in fragility. A comprehensive analysis requires information on building characteristics, including year of construction, as well as fragility curves and their change over time. Forecasts and scenarios analysing the area at different points in the future are also possible.

5 Conclusion

The approach developed for the derivation of fragility curves (Kohns et al. 2022) can be used to take into account the effects of ageing, including corrosion and pre-damage. When analysing existing buildings, the material and reinforcement properties are taken into account in accordance with the standard applicable at the year of construction. The main conclusions are as follows:

- The case study presented shows that corrosion attack can result in a 64% reduction in the overall shear base and an increase in fragility of up to 33% for an 80-year-old building constructed in 1943 compared to a new building constructed in 2023. The present study has demonstrated that utilising the loading and unloading method for analysing pre-damage can result in a maximal increase of 18% in the probability of exceedance, contingent on the extent of pre-damage and the damage grade sustained.
- The findings of the investigations conducted indicate that the individual aspects of ageing each result in a substantial increase in fragility. A further increase in fragility is anticipated when these aspects are combined.
- The application of fragility curves, developed for new buildings, results in a substantial underestimation of fragility when employed in relation to existing structures. The prototype application demonstrates the development of increasing fragility in buildings of varying ages.

Visualisations, such as the prototype application shown using a representative sample of streets and houses, can be automated and integrated with existing exposure models to provide estimates of the trend in fragility. A comprehensive analysis requires information on building characteristics, including year of construction, as well as fragility curves and their change over time. In addition, forecasts and scenarios can be produced that analyse the area at different points in the future. These can be used to support decisions by local authorities.

Author contributions Conceptualization: Julia Eberl, Alexander Stark; Methodology: Julia Eberl; Formal analysis and investigation: Julia Eberl; Software and Visualization: Julia Eberl; Validation: Julia Eberl, Alexander Stark; Writing - original draft preparation: Julia Eberl; Writing - review and editing: Julia Eberl, Alexander Stark; Supervision: Alexander Stark. All authors read and approved the final manuscript.

Funding Open Access funding enabled and organized by Projekt DEAL. The background research for this work was funded by the Federal Ministry of Education and Research (BMBF), Germany, in the framework of the project LOKI (FKZ: 03G0890E). The financial support is greatly appreciated by the authors.

Data availability The data analysed during the current study are available from the corresponding author on reasonable request.

Declarations

Competing interests The authors declare that they have no known competing financial or non-financial interests or personal relationships that could have appeared to influence the work reported in this paper.

References

Abdelnaby AE, Elnashai AS (2015) Numerical modeling and analysis of RC frames subjected to multiple earthquakes. Earthquakes Struct 9(5):957–981. https://doi.org/10.12989/eas.2015.9.5.957

Amadio C, Fragiacomo M, Rajgelj S (2003) The effects of repeated earthquake ground motions on the non-linear response of SDOF systems. Earthq Eng Struct Dynamics 32(2):291–308. https://doi.org/10.1002/eqe.225

Apostolopoulos CA, Papadakis VG (2008) Consequences of steel corrosion on the ductility properties of reinforcement bar. Constr Build Mater 22(12):2316–2324. https://doi.org/10.1016/j.conbuildmat.2007.10.006

Berto L, Vitaliani R, Saetta A et al (2009) Seismic assessment of existing RC structures affected by degradation phenomena. Struct Saf 31(4):284–297. https://doi.org/10.1016/j.strusafe.2008.09.006

Berto L, Caprili S, Saetta A et al (2020) Corrosion effects on the seismic response of existing rc frames designed according to different building codes. Eng Struct 216:110397. https://doi.org/10.1016/j.engstruct.2020.110397

Brzev S, Scawthorn C, Charleson AW et al (2013) GEM building taxonomy version 2.0: GEM technical report 2013-02 V1.0.0. https://doi.org/10.13117/GEM.EXP-MOD.TR2013.02

Capozucca R, Cerri M (2003) Influence of reinforcement corrosion–in the compressive zone–on the behaviour of RC beams. Eng Struct 25(13):1575–1583. https://doi.org/10.1016/S0141-0296(03)00119-6

Caprili S, Mattei F, Salvatore W (2024) Corrosion effects on the dissipative performance of critical regions of RC frame systems. Eng Struct 300:117259. https://doi.org/10.1016/j.engstruct.2023.117259

Celarec D, Vamvatsikos D, Dolsek M (2011) Simplified estimation of seismic risk for reinforced concrete buildings with consideration of corrosion over time. Bull Earthq Eng 9(4):1137–1155. https://doi.org/10.1007/s10518-010-9241-3

Centre for Research on the Epidemiology of Disasters, United Nations Office for Disaster Risk Reduction (2020) Human cost of disasters: an overview of the last 20 years 2000–2019. http://www.undrr.org/quick/50922

Coronelli D, Gambarova P (2004) Structural Assessment of Corroded Reinforced Concrete Beams: Modeling Guidelines. J Struct Eng 130(8):1214–1224. https://doi.org/10.1061/(ASCE)0733-9445(2004)130:8(1214)

Cosenza E, de Cicco F, Prota A (2010) Discussion of "Nonlinear Uniaxial Material Model for Reinforcing Steel Bars" by Sashi K. Kunnath, YeongAe Heo, and Jon F. Mohle. Journal of Structural Engineering 136(7):917–918. https://doi.org/10.1061/(ASCE)ST.1943-541X.0000119

Crowley H, Dabbeek J, Despotaki V et al (2021a) European seismic risk model (ESRM20): EFEHR technical report 002 V1.0.0. https://doi.org/10.7414/EUC-EFEHR-TR002-ESRM20

Crowley H, Silva V, Martins L et al (2021b) Open models and software for assessing the vulnerability of the European building stock. In: COMPDYN 2021: 8th ECCOMAS Thematic Conference on Computational Methods in Structural Dynamics and Earthquake Engineering. Institute of Structural Analysis and Antiseismic Research School of Civil Engineering Athens (NTUA), pp 2678–2688. https://doi.org/10.7712/120121.8666.19367

D'Ayala D, Meslem A, Vamvatsikos D et al (2015) Guidelines for analytical vulnerability assessment - low/mid-rise buildings: vulnerability global component project. https://doi.org/10.13117/GEM.VULN-MOD.TR2014.12

Deutscher Ausschuss für Eisenbeton (1937) Bestimmungen des Deutschen Ausschusses für Eisenbeton 1932 - A. Bestimmungen für Ausführung von Bauwerken aus Eisenbeton: DIN 1045 3. Ausgabe 05-1937

Di Sarno L (2013) Effects of multiple earthquakes on inelastic structural response. Eng Struct 56:673–681. https://doi.org/10.1016/j.engstruct.2013.05.041

Eberl J (2025) Fragilitätsuntersuchungen und Schadensklassifikationen im Erdbebenfall auf Basis von luftgestützten Aufnahmen. PhD Thesis, Karlsruher Institut für Technologie (KIT). https://doi.org/10.5445/KSP/1000176341

Faisal A, Majid TA, Hatzigeorgiou GD (2013) Investigation of story ductility demands of inelastic concrete frames subjected to repeated earthquakes. Soil Dyn Earthq Eng 44:42–53. https://doi.org/10.1016/j.soildyn.2012.08.012

Hatzigeorgiou GD, Beskos DE (2009) Inelastic displacement ratios for SDOF structures subjected to repeated earthquakes. Eng Struct 31(11):2744–2755. https://doi.org/10.1016/j.engstruct.2009.07.002

Hatzigeorgiou GD, Liolios AA (2010) Nonlinear behaviour of RC frames under repeated strong ground motions. Soil Dyn Earthq Eng 30(10):1010–1025. https://doi.org/10.1016/j.soildyn.2010.04.013

Hosseinpour F, Abdelnaby AE (2017) Effect of different aspects of multiple earthquakes on the nonlinear behavior of RC structures. Soil Dyn Earthq Eng 92:706–725. https://doi.org/10.1016/j.soildyn.2016.11.006

Jeon JS (2013) Aftershock vulnerability assessment of damaged reinforced concrete buildings in California. Dissertation, Georgia Institute of Technology, Atlanta, United States

Jeon JS, DesRoches R, Lowes LN et al (2015) Framework of aftershock fragility assessment–case studies: older California reinforced concrete building frames. Earthq Eng Struct Dynamics 44:2617–2636. https://doi.org/10.1002/eqe.2599

Kohns J, Stempniewski L, Stark A (2022) Fragility functions for reinforced concrete structures based on multiscale approach for earthquake damage criteria. Buildings 12(8). https://doi.org/10.3390/buildings12081253

Kohns J, Stempniewski L, Stark A (2023) Berücksichtigung von Alterungseffekten bei der Entwicklung von Fragilitätskurven für Stahlbetongebäude. In: Wuttke F, Aji HD, Özarmut A (eds) Tagungsband der 18. D-A-CH-Tagung Erdbebeningenieurwesen und Baudynamik. p 93–100

Kohns J, Zahs V, Klonner C et al (2025) Building Damage Assessment in Natural Disasters: A Trans- and Interdisciplinary Approach Combining Domain Knowledge, 3D Machine Learning, and Crowdsourcing. Progress Disaster Sci 26:100427. https://doi.org/10.1016/j.pdisas.2025.100427

LOKI Project Team (2023a) LOKI GitLab-Project. URL https://git.gfz-potsdam.de/loki

LOKI Project Team (2023b) Wiki - LOKI – Luftgestützte Observation Kritischer Infrastrukturen. URL https://git.gfz-potsdam.de/loki/lokiwiki

Luco N, Bazzurro P, Cornell CA (2004) Dynamic versus static computation of the residual capacity of a mainshock-damaged building to withstand an aftershock. In: 13th World Conference on Earthquake Engineering. No. 2405, Vancouver, B.C., Canada

Luzi L, Puglia R, Russo E et al (2015) Engineering strong motion database (ESM), version 1.0. https://doi.org/10.13127/ESM

Martins L, Silva V (2021) Development of a fragility and vulnerability model for global seismic risk analyses. Bull Earthq Eng 19:6719–6745. https://doi.org/10.1007/s10518-020-00885-1

Martins L, Silva V, Crowley H et al (2021) Vulnerability modellers toolkit, an open-source platform for vulnerability analysis. Bull Earthq Eng 19:5691–5709. https://doi.org/10.1007/s10518-021-01187-w

Menegotto M, Pinto P (1973) Method of analysis for cyclically loaded R.C. plane frames including changes in geometry and non-elastic behaviour of elements under combined normal force and bending. Symp Resist Ultimate Deformability Struct Acted Well Defined Repeated Loads 15–22. https://doi.org/10.5169/SEALS-13741

Pitilakis KD, Karapetrou ST, Fotopoulou SD (2014) Consideration of aging and SSI effects on seismic vulnerability assessment of RC buildings. Bull Earthq Eng 12:1755–1776. https://doi.org/10.1007/s10518-013-9575-8

Raghunandan M, Liel AB, Luco N (2015) Aftershock collapse vulnerability assessment of reinforced concrete frame structures. Earthq Eng Struct Dynamics 44:419–439. https://doi.org/10.1002/eqe.2478

Rodriguez J, Andrade C (2001) CONTECVET - A validated users manual for assessing the residual service life of concrete structures: Manual for assessing corrosion-affected concrete structures

Rodriguez J, Ortega LM, Casal J (1997) Load Carrying Capacity of Concrete Structures with Corroded Reinforcement. Constr Build Mater 11(4):239–248

Ruiz-Garcia J (2012) Mainshock-Aftershock Ground Motion Features and Their Influence in Building's Seismic Response. J Earthquake Eng 16:719–737. https://doi.org/10.1080/13632469.2012.663154

Ruiz-Garcia J, Aguilar JD (2015) Aftershock seismic assessment taking into account postmainshock residual drifts. Earthq Eng Struct Dynamics 44:1391–1407. https://doi.org/10.1002/eqe.2523
Seismosoft (2023) SeismoStruct 2023 – A computer program for static and dynamic nonlinear analysis of framed structures. https://seismosoft.com/
Silva V, Henshaw P, Huyck C et al (2018) GED4ALL - Global exposure database for multi-hazard risk analysis: D5 - Final report, GEM technical report 2018-05
Silva V, Calderon A, Todorovic L et al (2022) Incorporating future earthquake risk in disaster risk management. In: Vacareanu R, Ionescu C (eds) Progresses in European Earthquake Engineering and Seismology. Springer Proceedings in Earth and Environmental Sciences, Springer International Publishing, Cham, p 179–196. https://doi.org/10.1007/978-3-031-15104-0
Simioni P (2009) Seismic response of reinforced concrete structures affected by reinforcement corrosion. Dissertation, University of Braunschweig and University of Florence
SYNER-G (2011) Systemic seismic vulnerability and risk analysis for buildings, lifeline networks and infrastructure safety gain: D3.1 - Fragility functions for common. RC building types in Europe
Vecchio FJ, Collins MP (1986) The modified compression-field theory for reinforced concrete elements subjected to shear. ACI J 1986;83(2):219–231
Wen W, Zhai C, Ji D et al (2017) Framework for the vulnerability assessment of structure under mainshock-aftershock sequences. Soil Dyn Earthq Eng 101:41–52. https://doi.org/10.1016/j.soildyn.2017.07.002
Yalciner H, Sensoy S, Eren O (2012) Time-dependent seismic performance assessment of a single-degree-of-freedom frame subject to corrosion. Eng Fail Anal 19:109–122. https://doi.org/10.1016/j.engfailanal.2011.09.010
Zahs V, Kohns J, Meyer F et al (2023) LOKI – Luftgestützte Observation Kritischer Infrastrukturen: Schlussbericht, Berichtszeitraum: 01.01.2020–31.03.2023. https://doi.org/10.2314/KXP:1885697937
Zhai C, Wen W, Li S et al (2014) The damage investigation of inelastic SDOF structure under the mainshock–aftershock sequence-type ground motions. Soil Dyn Earthq Eng 59:30–41. https://doi.org/10.1016/j.soildyn.2014.01.003